Physica D 239 (2010) 547 560

Contents lists available at ScienceDirect

Physica D

journal homepage: www.elsevier.com/locate/physd

Effects of synaptic depression and adaptation on spatiotemporal dynamics of an excitatory neuronal network

Zachary P. Kilpatrick [a], Paul C. Bressloff [a,b,*]

[a] Department of Mathematics, University of Utah, Salt Lake City, UT 84112, USA

[b] Mathematical Institute, University of Oxford, 24-29 St. Giles', Oxford OX1 3LB, UK

a r t i c l e i n f o

Article history:
Available online 13 June 2009

Keywords:
Excitatory neuronal network
Synaptic depression
Spike frequency adaptation
Self-sustained oscillations

a b s t r a c t

We analyze the spatiotemporal dynamics of a system of integro-differential equations that describes a one-dimensional excitatory neuronal network with synaptic depression and spike frequency adaptation. Physiologically suggestive forms are used for both types of negative feedback. We also consider the effects of employing two different types of firing rate function, a Heaviside step function and a piecewise linear function. We first derive conditions for the existence of traveling fronts and pulses in the case of a Heaviside step firing rate, and show that adaptation plays a relatively minor role in determining the characteristics of traveling waves. We then derive conditions for the existence and stability of stationary pulses or bumps, and show that a purely excitatory network with synaptic depression cannot support stable bumps. However, bumps do not exist in the presence of adaptation. Finally, in the case of a piecewise linear firing rate function, we show numerically that the network also supports self-sustained oscillations between an Up state and a Down state, in which a spatially localized oscillating core periodically emits pulses at each cycle.

1. Introduction

Large scale neuronal networks can exhibit a number of spatially structured activity states *in vivo* and *in vitro*, which may be observed experimentally using multi-electrode arrays or voltage-sensitive dye imaging [1]. When neocortical or hippocampal *in vitro* slices are treated with an inhibitory neurotransmitter antagonist such as bicuculline, effectively eliminating inhibition, a localized current stimulus evokes population activity. Such activity may take the form of a spatially localized group of neurons whose population activity oscillates around 1 10 Hz [2,3], and each oscillation cycle may emit elevated activity that propagates as a traveling pulse [2,4,5] or even a spiral wave [6]. A variety of sensory stimuli have been linked to propagating waves *in vivo*. For example, a number of studies of vertebrate and invertebrate olfactory bulbs have shown odor stimuli can elicit oscillations and propagating waves [7,8]. Similarly, a small visual stimulus can evoke a propagating wave in the visual cortex [9 12], and stimulating a single whisker can trigger a wave in the rat barrel cortex [13]. Spatiotemporal activity is not only a neural correlate of sensory stimuli, but can also precede motor commands. For example, evoked waves have been found in monkey motor cortex during movement preparation and execution [14]. Finally, stationary waves or bumps of persistent spatial activity that neither propagate nor oscillate have been seen during working memory tasks [15].

Oscillations and traveling waves can also be the signature of certain brain pathologies such as epilepsy [3]. Electrophysiology has been used to study epilepsy in humans as well as animal models, and seizures are usually accompanied by measurable structured population activity. In fact, the nature of such structured population activity as recorded by electroencephalogram can indicate the nature of the seizure mechanism [16]. As in cortical slice studies, some seizures have hallmark electrical activity traces consisting of focused localized synchronous oscillations that emit traveling pulses [3]. Thus, it is useful to understand the mechanisms behind population oscillations and traveling waves in large scale neuronal networks due to their important functional and pathological implications. A number of organizing mechanisms for such spatiotemporal activity have been suggested, including a single pacemaker oscillator exciting successive neighbors in an excitable network, or coupled oscillators propagating gradual phase delays in space [17,5].

In many slice experiments, inhibitory connectivity is pharmacologically blocked so that any negative feedback in the network is likely to arise at the single cell level due to mechanisms such as spike frequency adaptation or synaptic depression. Spike frequency adaptation causes a neuron's firing rate to decay to a submaximal level and occurs when a potassium current, presumably activated by elevated

* Corresponding author at: Mathematical Institute, University of Oxford, 24-29 St. Giles', Oxford OX1 3LB, UK.
E-mail addresses: kilpatri@math.utah.edu (Z.P. Kilpatrick), bresslof@math.utah.edu (P.C. Bressloff).

0167-2789/$ see front matter
doi:10.1016/j.physd.2009.06.003

intracellular calcium, hyperpolarizes the membrane [18 20]. This so called afterhyperpolarization current has been shown via both experimental and modeling studies to have a time constant around 40 120 ms and to reduce the firing rate by about 1=3 [18 22]. Synaptic depression is the process by which resources are depleted in the presynaptic bouton [23]. These resources may be scaffolding proteins that participate in exocytosis, synaptic vesicles, or excitatory neurotransmitter like glutamate. They are depleted with a time constant comparable to the membrane time constant of around 10 ms, but they recover much more slowly over an interval of 200 800 ms [24 27]. The firing rate of a neuron receiving a sustained input can reduce to as little as 5% 10% of the initial rate over 100 ms [24,25,28]. The details of both forms of negative feedback, including their associated time constants, are likely to be important in determining conditions for the existence and stability of spatially structured activity states such as traveling waves, standing bumps, or focused oscillations.

Recent theoretical studies of the role of negative feedback in neuronal network spatiotemporal dynamics have mainly been based on a neural field model with linear negative feedback introduced by Pinto and Ermentrout [29,30,6,31 39]:

$$\frac{@u.x; t/}{@t} = -u.x; t/ + \int_{-\infty}^{\infty} w.x; x'/H.u.x'; t/ - /\mathrm{d}x' - a.x; t/ + I.x; t/; \tag{1.1}$$

$$\frac{@a.x; t/}{@t} = u.x; t/ - a.x; t/; \tag{1.2}$$

where u is synaptic input current, w represents the synaptic weighting between neurons, H is a Heaviside firing rate function with the firing threshold, $I.x; t/$ is an external input, a is a slow local negative feedback component and and are the time constant and strength of the feedback, respectively. Pinto and Ermentrout established that for zero input and large enough negative feedback, traveling pulses exist. More recent extensions of this work have explored various scenarios for the occurrence of spatiotemporal oscillations. For example, Folias and Bressloff have shown that in the presence of a localized Gaussian input I, standing and traveling pulses of activity can transition to spatially localized oscillators or breathers, which can then act as wave emitters [31 33]. On the other hand, Troy and Shusterman [36] have shown that for large enough negative feedback , a low activity state corresponding to a homogeneous fixed point of Eqs. (1.1) and (1.2) for $I = 0$ has complex eigenvalues that lead to multi-pulse solutions. When simulated in two dimensions, the spatially extended system supports a re-entrant localized rotor that periodically emits target waves (see also [6,35]). In a subsequent study, they showed that making even larger can lead to a stable limit cycle about the low activity state [38]. Thus, in one dimension, periodic oscillations emit a traveling pulse at each cycle mimicking EEG data of epileptic seizures [3]. Coombes and Owen have recently introduced a nonlinear model of negative feedback [40] in which the firing threshold is treated as the adaptation variable, and have shown that this leads to a variety of spatiotemporal dynamics including breathers and more exotic solutions.

In this paper, we analyze the spatiotemporal dynamics of a neural field model that takes into account two physiologically based forms of nonlinear negative feedback, namely, spike frequency adaptation and synaptic depression. The basic model is introduced in Section 2. We then derive conditions for the existence of traveling fronts and pulses in the case of a Heaviside firing rate function (see Section 3). We show that adaptation plays a relatively minor role in determining the characteristics of the waves. For example, the wavespeed of a propagating front is independent of the adaptation parameters, whilst both the width and speed of a traveling pulse are only weakly dependent on adaptation. As in the case of linear adaptation [29], there coexists a stable branch of fast/wide pulses and an unstable branch of slow/narrow pulses. The existence and stability of standing pulses or bumps is analyzed in Section 4, where we show that care has to be taken in treating a discontinuous firing rate function. Finally, in Section 5, we consider a more realistic piecewise linear firing rate function for which self-sustained oscillations can occur; these oscillations persist in the absence of adaptation.

2. Neural field model with synaptic depression and spike frequency adaptation

We consider a neural network model which include two forms of negative feedback, synaptic depression [26,41 43] and spike frequency adaptation [18 20]. As opposed to the usual Pinto Ermentrout formulation of negative feedback in spatially extended neural fields [29,36,39], our negative feedback accounts for two separate physiological mechanisms, both of which depend on the output firing rate f. Hence, Eqs. (1.1) and (1.2) are modified according to the following system of equations:

$$\frac{@u.x; t/}{@t} = -u.x; t/ + \int_{-\infty}^{\infty} w.x; x'/q.x'; t/f.u.x'; t/ - a.x'; t//\mathrm{d}x'; \tag{2.1a}$$

$$\frac{@q.x; t/}{@t} = \frac{1 - q.x; t/}{} - q.x; t/f.u.x; t/ - a.x; t//; \tag{2.1b}$$

$$\frac{@a.x; t/}{@t} = -a.x; t/ + f.u.x; t/ - a.x; t//: \tag{2.1c}$$

Eq. (2.1a) describes the evolution of the synaptic current $u.x; t/$ in the presence of synaptic depression and spike frequency adaptation, which take the form of a synaptic scaling factor $q.x; t/$ evolving according to Eq. (2.1b) and an outward hyperpolarizing adaptation current $a.x; t/$ evolving according to Eq. (2.1c). The factor $q.x; t/$ can be interpreted as a measure of available presynaptic resources, which are depleted at a rate f [26,41,43], and are recovered on a timescale specified by the constant which is experimentally shown to be 200 800 ms [24 26]. Suppose that we fix parameters such that f is interpreted as the fraction of the maximum firing rate, that is $0 \leq f \leq 1$. If we assume that the strength of a synapse is reduced by a factor $= 0{:}05$ $0{:}4$ of its maximal value in response to a sustained input of rate $f = 1$ [24], then a simple steady-state calculation shows that $\approx .1 - /=. / \approx 0{:}003 - 0{:}1\ .\mathrm{ms}/^{-1}$ for the given range of values of . The adaptation current $a.x; t/$ is activated with strength and time constant (experimentally shown to be 40 120 ms [19,20]). As derived from a universal adaptation current by Benda and Herz [18], spike frequency adaptation is switched on as a linear function of a neuron's firing rate.[1]

[1] Our model of adaptation differs from Coombes and Owen [40], who take the nonlinear part of Eq. (2.1c) to be of the form $f.u.x; t/ - /$ for a fixed .

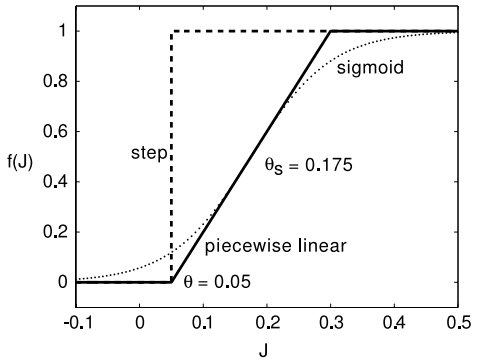

Fig. 1. Comparison of the step, piecewise linear, and sigmoid firing rate functions. Parameter values are $= 0{:}05$ and $= 4$. The sigmoid function has the same slope and value as the piecewise linear function at their mean values. When compared to the sigmoid function, it is apparent that the piecewise linear function's true threshold is more accurately given by $_s = 0{:}175$, rather than , the point at which nonzero firing occurs.

Following Amari's original work on scalar networks [44], most analytical studies of the Pinto Ermentrout model take the nonlinear firing-rate function f to be a Heaviside step function [29,30,38,31 33,36,39] (although see [45] for a functional analytic study of neural field models with smooth nonlinearities):

$$f(J) = H(J -) = \begin{cases} 0; & J \in (-\infty;); \\ 1; & J \in [; \infty). \end{cases} \tag{2.2}$$

We will use such a function in order to study the existence and stability of traveling waves and bumps (see Sections 3 and 4). However, as we show in Section 5, a network with synaptic depression can only support self-sustained oscillations if we consider a more general firing rate function such as the piecewise linear function (see Fig. 1)

$$f(J) = \begin{cases} 0; & J \in (-\infty;); \\ (J -)/; & J \in (; + ^{-1}/); \\ 1; & J \in [+ ^{-1}; \infty). \end{cases} \tag{2.3}$$

(One could also consider a firing rate function with a step followed by linear increase [46,47]). Here specifies the slope or gain of the firing rate function such that in the limit $\to \infty$, we recover the step function (2.2). Note that taking the firing rate to be a linear function close to threshold is consistent with the observation that spike frequency adaptation tends to linearize the firing frequency-input current curve [21,22]. One important point is that even if the firing threshold is the same in Eqs. (2.3) and (2.2), a more intuitive threshold for the piecewise linear function should match the half height threshold $_s$ usually defined for the sigmoidal function

$$f (J) = \frac{1}{1 + e^{- (J - s)}} \tag{2.4}$$

as illustrated in Fig. 1. Treating the Heaviside function as the high gain limit of a sigmoid also implies that $H(0) = 1=2$. The value of the Heaviside function at zero plays a subtle but crucial role in the stability analysis of bumps, since the steady-state distribution of the depression variable is discontinuous (see Section 4).

Finally, we take the excitatory weight function w to be a normalized exponential,

$$w(x; x') = \frac{1}{2d} e^{-|x - x'|=d}; \tag{2.5}$$

where d is the effective range of the excitatory distribution. We fix the temporal and spatial scales of the network by setting $= 1, d = 1$. The membrane time constant is typically around 10 ms and the length-scale of synaptic connections is typically 1 mm. Since the weight function is symmetric, depending only on the Euclidean distance, we can write $w(x; x') = w(|x - x'|)$.

3. Traveling waves

Several experimental studies of disinhibited cortical slices and *in vivo* cortical regions have exhibited traveling fronts and pulses of superthreshold activity [2,5,6,10]. Neural field models of excitatory networks have sought to give heuristic explanations of such phenomena from a dynamical systems point of view [29,31,32,40,36,38,39]. In this section we present to our knowledge the first neural field study of traveling waves in a spatially extended network that includes physiologically justified terms for both synaptic depression and spike frequency adaptation. In the case of the step firing rate function (2.2), we can carry out the analysis along similar lines to previous modeling studies. We look for solutions to the system (2.1), $u(x; t) = U( ), q(x; t) = Q( ), a(x; t) = A( )$, where $= x - ct$ is the traveling wave coordinate.

3.1. Fronts

We specify conditions for a traveling front in our neural field model as follows. The total current $J( ) = U( ) - A( )$ must cross the threshold of the activation function at exactly one point. We can conveniently fix this point to be $= 0$ due to translation invariance.

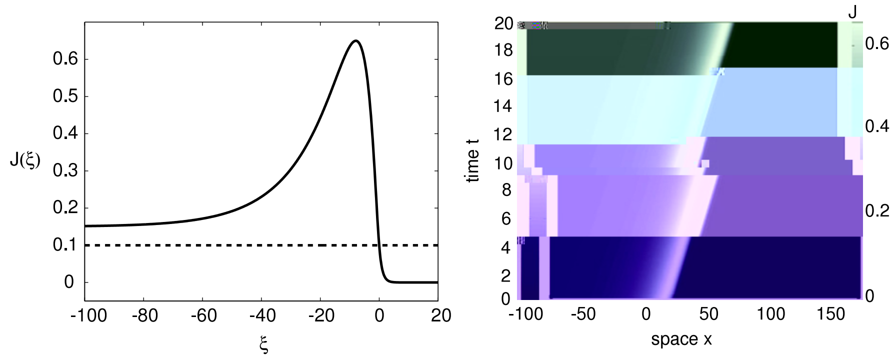

Fig. 2. (Left) Profile of analytical front solution $J(\ ) = U(\ ) - A(\ )$ for parameter values $\ = 0.1$, $\ = 20$, $\ = 0.2$, $\ = 5$, and $\ = 0.05$. Wavespeed c_+ is specified by Eq. (3.15). Note that, as $\ \to -\infty$, $J(\ ) \to 1/(1 + \ \ ) - \ $. (Right) Corresponding space time plot of a traveling front obtained by solving the system (2.1) numerically with the analytical front solution taken as the initial condition.

For concreteness, we consider a right moving front by taking the current J to be superthreshold (subthreshold) to the left (right) of $\ = 0$. We then have

$$J(\ ) = U(\ ) - A(\ ) = \ ; \quad \text{at} \quad \ = 0; \tag{3.1}$$

$$J(\ ) = U(\ ) - A(\ ) ? \ ; \quad \text{for} \quad \ 7\ 0; \tag{3.2}$$

$$\{U(\ ); Q(\ ); A(\ )\} \to \{0; 1; 0\}; \quad \text{as} \quad \ \to \infty; \tag{3.3}$$

$$c \geq 0. \tag{3.4}$$

It follows from our model system (2.1) that such a traveling front will evolve according to

$$-cU'(\ ) = -U(\ ) + \int_{-\infty}^{0} Q(\ ')w(|\ - \ '|)d\ '; \tag{3.5}$$

$$-c\ Q'(\ ) = 1 - Q(\ ) - \ Q(\ )\ (- \ ); \tag{3.6}$$

$$-c\ A'(\ ) = -A(\ ) + \ (- \ ); \tag{3.7}$$

where

$$(\ ) = \begin{cases} 1; & \geq 0; \\ 0; & < 0. \end{cases} \tag{3.8}$$

Eqs. (3.6) and (3.7) can be solved explicitly to give

$$Q(\ ) = \begin{cases} 1; & \text{for} \quad > 0; \\ \dfrac{1}{1 + \ }\left(1 + \ e^{(1+\ )\ /\ c}\right); & \text{for} \quad \leq 0 \end{cases} \tag{3.9}$$

and

$$A(\ ) = \begin{cases} 0; & \text{for} \quad > 0; \\ (1 - e^{\ /c}); & \text{for} \quad \leq 0. \end{cases} \tag{3.10}$$

Substituting (3.9) back into (3.5), we have

$$-cU'(\ ) = -U(\ ) + F(\ ); \tag{3.11}$$

$$F(\ ) = \frac{1}{1 + \ } \int_{-\infty}^{0} \left(1 + \ e^{(1+\ )\ '/\ c}\right) w(|\ - \ '|)d\ '. \tag{3.12}$$

In the case of an exponential weight function, we can explicitly evaluate $F(\ )$ and thus solve Eq. (3.11) after imposing the appropriate asymptotic behavior. The threshold condition $J(0) = U(0) - A(0) = \ $ then leads to the following relationship between front speed c and the threshold $\ $:

$$= \frac{(c \ + 1)}{2(c + 1)(c \ + (1 + \ ))}. \tag{3.13}$$

A front solution is shown in Fig. 2.

We can derive an explicit expression for the wavespeed c in terms of other parameters from (3.13) by finding the roots of the quadratic

$$2 \ c^2 + (2 \ (\ + (1 + \ )) - \ )c + 2 \ (1 + \ ) - 1 = 0; \tag{3.14}$$

which are

$$c_{\pm} = \frac{1}{4} \left(-2 \ (\ + (1 + \ )) \pm \sqrt{\mathcal{D}} \right); \tag{3.15}$$

$$\mathcal{D} = \ ^2 - 4 \ (\ + (1 + \ )) + 4 \ ^2(\ + (1 + \ ))^2 - 16 \ ^2(1 + \ ) + 8 \ . \tag{3.16}$$

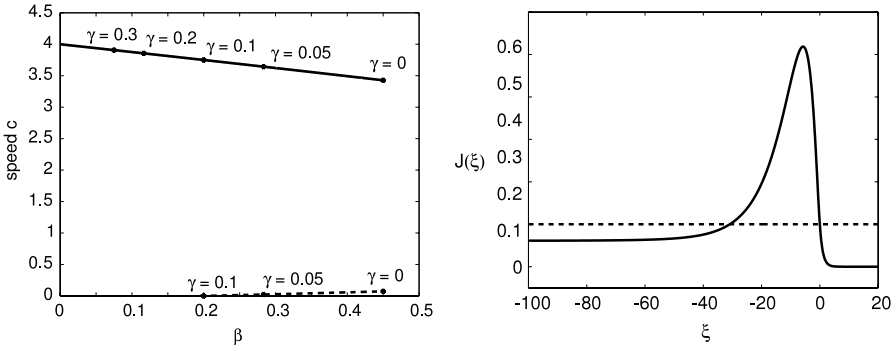

Fig. 3. (Left) Dispersion curve of wavespeed c_+ (solid) and c_- (dashed) versus depression strength . Numerical results show the fast front (c_+) is stable and the slow front (c_-) is unstable. The maximal value of for which the superthreshold condition (3.17) is satisfied is given by a dot on each dispersion curve for a particular value of . Parameters are = 0.1, = 20, and = 5. (Right) A front that violates the superthreshold condition (3.17), despite its construction being specified by all other conditions. When the system (2.1) is solved numerically with such an initial condition, the solution settles into a traveling pulse.

In order for a front to exist with wavespeed $c_\pm$ as we have constructed it, $c_\pm$ must be real and nonnegative. None of the adaptation parameters or enter into the dispersion relation for fronts. However, in order for a front to exist, we must also satisfy $J(\ )>$ for <0 as given by (3.2) to make sure the trailing edge of the front does not cross back below threshold as identified in a similar analysis in [36]. Therefore, we impose the necessary condition

$$\lim_{\to-\infty}[U(\ )-A(\ )]=\frac{1}{1+}-\quad>\quad\Longrightarrow\quad<\frac{1}{1+}-\ ;\qquad<\frac{1}{(\ )+}-\frac{1}{}: \tag{3.17}$$

Otherwise, the trailing edge of the front dips below threshold, the superthreshold region has finite width, and therefore the profile evolves into a pulse. We quantify the dependence of wavespeed c on synaptic depression parameters in Fig. 3.

3.2. Pulses

For a traveling pulse, the total current $J(\ )=U(\ )-A(\ )$ must cross the threshold of the activation function at exactly two points. Once again, fix these points to be $=-\ ;0$. Total current J must be superthreshold between these two points, and subthreshold otherwise. Imposing this, as well as reasonable boundary conditions, we have

$$J(\ )=U(\ )-A(\ )=\ ;\quad\text{at}\quad=-\ ;0; \tag{3.18}$$

$$J(\ )=U(\ )-A(\ )>\ ;\quad\text{for}\quad\in(-\ ;0); \tag{3.19}$$

$$J(\ )=U(\ )-A(\ )<\ ;\quad\text{for}\quad\in(-\infty;-\ )\cup(0;\infty); \tag{3.20}$$

$$U(\ )-A(\ )\to 0;\quad\text{as}\quad\to\pm\infty; \tag{3.21}$$

$$Q(\ )\to 1;\quad\text{as}\quad\to\pm\infty: \tag{3.22}$$

Thus, it follows from our system (2.1) that such a traveling pulse will evolve according to

$$-cU'(\ )=-U(\ )+\int_{-}^{0}Q(\ ')w(|-\ '|)\,d\ '; \tag{3.23}$$

$$-c\ Q'(\ )=1-Q(\ )-\ Q(\ )(\ -)+\ (\ -\ -\ ); \tag{3.24}$$

$$-c\ A'(\ )=-A(\ )+\ (\ -)+\ (\ -\ -\ ); \tag{3.25}$$

As in the front case, we can solve the system of equations by solving Eqs. (3.24) and (3.25) individually, and then plugging $Q(\ )$ back into Eq. (3.23). Using integrating factors, we find that

$$Q(\ )=\begin{cases}1; & >0;\\ \dfrac{1}{1+}\,1+\ e^{(1+)(\ )/c}; & \in(-\ ;0);\\ 1-\dfrac{}{1+}\,e^{-(\ +)/c}-e^{(1+)(\ )/c}; & <-\end{cases} \tag{3.26}$$

and

$$A(\ )=\begin{cases}0; & >0;\\ 1-e^{-(\ )/c}; & \in(-\ ;0);\\ e^{-(\ )/c}-1\ e^{-(\ )/c}; & <-\ :\end{cases} \tag{3.27}$$

Substituting (3.26) back into (3.23),

$$-cU'(\ )=-U(\ )+G(\ ); \tag{3.28}$$

$$G(\ )=\frac{1}{1+}\int_{-}^{0}1+\ e^{(1+)(\ )/c}\,w(|-\ '|)\,d\ ': \tag{3.29}$$

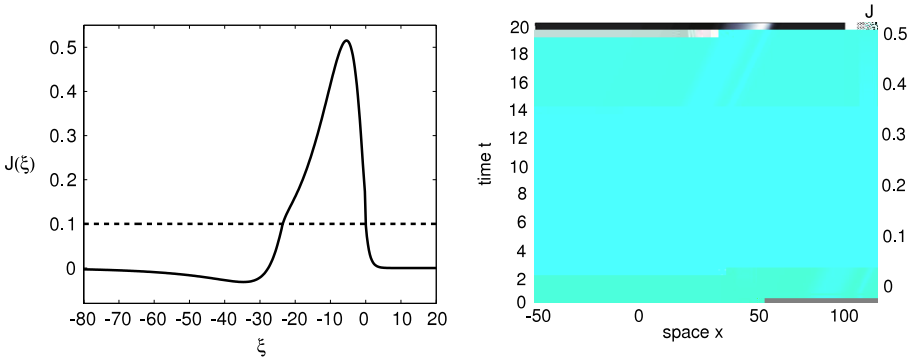

Fig. 4. (Left) Profile of a pulse solution $J. / = U. / - A. /$. Note that the solution remains above threshold within the region $\in . - ; 0/$. (Right) Corresponding space time plot of a traveling pulse obtained by numerically solving (2.1) with the analytical solution as the initial condition. Parameters are $= 20$, $= 0{:}4$, $= 5$, and $= 0{:}1$.

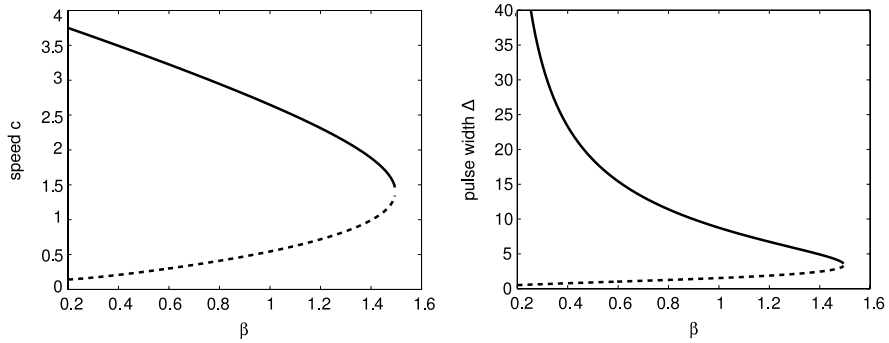

Fig. 5. Bifurcation curves for the existence of traveling pulses for the system (2.1) in (Left) the $(; c)$ and (Right) the $(;)$ plane. There exists a stable branch of fast/wide pulses (solid curves) and an unstable branch of slow/narrow pulses (dashed curves), which annihilate in a saddle node bifurcation. Parameter values are $= 0{:}1$, $= 20$, $= 5$, and $= 0{:}1$.

Notice that in the limit $\to \infty$, we recover the equation for $U. /$ in the front case. Again we can find the explicit solution for $U. /$ when $W.| - '|/$ is taken to be the exponential weight function. The threshold conditions $J.- / = J.0/ =$ then lead to the following pair of equations for the wavespeed c and pulsewidth .

$$= K_0 - K_1 e^{-} - K_2 e^{-.1+ / =.c /} e^{-} ; \tag{3.30}$$

$$= L_0 + L_1 e^{-} + L_2 e^{-.1+ / =.c /} - L_3 e^{- =c} + e^{- =.c /}; \tag{3.31}$$

where

$$K_0 = \frac{.c + 1/}{2.c + 1/.c + .1 + //}; \qquad K_1 = \frac{1}{2.c + 1/.1 + /};$$

$$K_2 = \frac{c^{2}}{2.c + 1/.1 + /.c + .1 + //};$$

$$L_0 = \frac{2c + 1}{2.c + 1/.1 + /} - ; \qquad L_1 = \frac{.c - 1/}{2.c - 1/.c - .1 + //};$$

$$L_2 = \frac{c^{2\ 4}}{.1 + /.c^{2\ 2} - .1 + /^2/. - .1 + //} - \frac{c^{2}}{2.c + 1/.1 + /.c + .1 + //};$$

$$L_3 = \frac{1}{1 +} \ 1 + \frac{c^{2\ 4}}{.c^{2\ 2} - .1 + /^2/. - .1 + //} + \frac{c^{2\ 2}.1 + / - .1 + /}{.c^2 - 1/.c^{2\ 2} - .1 + /^2/};$$

A pulse solution is shown in Fig. 4.

We cannot derive explicit expressions for $.c; /$ from (3.30) and (3.31), but we can solve them numerically using a root finding algorithm. Notice that adaptation parameters do enter into this system as they play a role in how quickly activity tails back down to subthreshold levels. We plot existence curves for traveling pulses as a function of in Fig. 5. Stable traveling pulses exist for small enough depression strength . As in the case of linear adaptation [29], there coexists a stable branch of fast/wide pulses and an unstable branch of slow/narrow pulses. We show similar existence curves as functions of the time constant in Fig. 6. Here, stable traveling pulses exist for slow enough synaptic depression. In general, the wavespeed c and pulsewidth are fairly insensitive to changes in or the time constant of adaptation despite their appearance in the dispersion relation. As in the case of traveling fronts (Section 3.1), it appears that adaptation has little influence on the character of traveling waves, aside from slightly modifying existence regions.

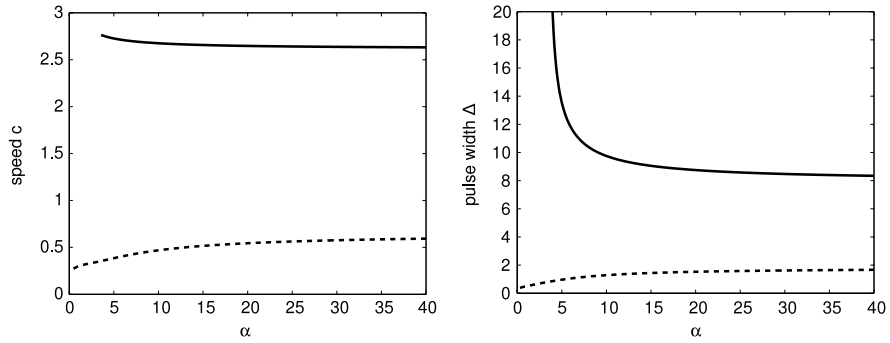

Fig. 6. Corresponding bifurcation curves for the existence of traveling pulses for the system (2.1) in (Left) the (; c) and (Right) the (;) plane. Stable (unstable) branches are indicated by solid (dashed) curves. Parameter values are = 0:1, = 0:9, = 5, and = 0:1.

4. Stationary pulses or bumps

Consistent with previous continuum neural field models, we show that negative feedback in the form of synaptic depression cannot generate stable stationary pulses or bumps in a homogeneous excitatory network. Thus some form of lateral inhibition [44,30,40] or external input [31,32] is required to stabilize the bump. (Rubin and Bose have shown that for a discrete network of type I oscillators with synaptic depression, stationary bumps could also be stabilized, but they did not explore the continuum case [48]).

4.1. Existence

In the case of a stationary (time-independent) bump solution, the total current $J.x/ = U.x/ - A.x/$ crosses threshold twice. We may fix these point to be $x = - \ ;0$, due to translation invariance. The total current J must be superthreshold between these two points and subthreshold otherwise. However, since depression and adaptation are activated by a discontinuous function $f \equiv H$, any threshold crossing will lead to a discontinuous change in $A.x/$, driving part of the interior back below threshold. In Section 3, it was shown that adaptation plays a minor role in describing traveling wave solutions of system (2.1). Here, stable stationary bumps are disrupted in numerical simulations by inclusion of arbitrarily small amounts of adaptation. Hence, we set $= 0$ and determine whether or not a stable bump can occur in the case of synaptic depression alone. Our conditions for a bump solution are as follows:

$$U.x/ = \ ; \quad \text{at } x = - \ ;0; \tag{4.1}$$

$$U.x/ > \ ; \quad \text{for } x \in .- \ ;0/; \tag{4.2}$$

$$U.x/ < \ ; \quad \text{for } x \in .-\infty;- \ /\cup .0;\infty/ \tag{4.3}$$

$$U.x/ \to 0; \quad \text{as } x \to \pm\infty; \tag{4.4}$$

$$Q.x/ \to 1; \quad \text{as } x \to \pm\infty: \tag{4.5}$$

The time-independent version of system (2.1) with $= 0$ then reduces to the pair of equations

$$U.x/ = \int_{-}^{0} Q.x'/w.|x - x'|/dx'; \tag{4.6}$$

$$Q.x/ = 1 + \ \frac{1}{1+} - 1 \ H.U.x/ - \ / \tag{4.7}$$

with $H.0/ = 1=2$. Substituting (4.7) into (4.6) and using an exponential weight function yields the solution

$$U.x/ = \begin{cases} \dfrac{1 - e^{-}}{2.1+ \ /} e^{-x}; & x > 0; \\ \dfrac{2 - e^{x} - e^{-x-}}{2.1+ \ /}; & x \in .- \ ;0/; \\ \dfrac{e \ - 1}{2.1+ \ /} e^{x}; & x < - \ : \end{cases} \tag{4.8}$$

Applying the threshold conditions $U.- \ / = U.0/ =$, we arrive at an implicit expression for the bump width

$$\frac{1 - e^{-}}{2.1+ \ /} = \ ; \tag{4.9}$$

which can be solved explicitly for

$$= - \ln[1 - 2 \ .1+ \ /]: \tag{4.10}$$

In order that be real and positive, we require

$$< \frac{1}{-} \ \frac{1}{2} - 1 \ : \tag{4.11}$$

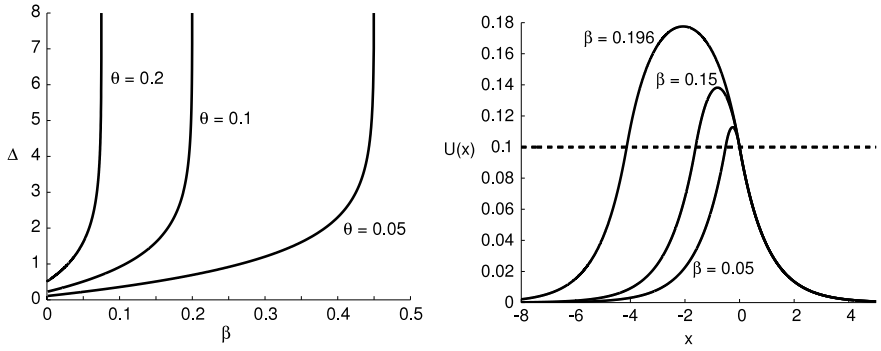

Fig. 7. (Left) Plots relating bump width to amplitude of synaptic depression for various values of threshold using Eq. (4.10). Beyond each curve's vertical asymptote value, no bumps exist for that particular value of . Changing merely serves to inversely scale the associated with a particular width; here = 20. (Right) Bump profiles when = 0:1 and = 20 for various values of . Smooth bumps satisfying all threshold conditions require adaptation to be nonexistent (= 0).

The variation of pulsewidth with the parameters and is shown in Fig. 7. Profiles of various bumps are also given. Note that bumps are always coexistent with fronts. The existence of stationary pulses has been proven before in the Pinto Ermentrout model [31,36], but such bumps are always unstable unless a sustained inhomogeneous input is also applied [31]. We will now show that bumps are also unstable in a homogeneous excitatory network with synaptic depression.

4.2. Stability

Rather than only considering perturbations of the threshold crossing points along the lines of Amari [44], we formally linearize about the bump solution in order to analyze the spectrum of the linear operator. However, considerable care must be taken in carrying out this ``linearization'', since the steady-state depression variable $Q(x)$ is a discontinuous function of x. In particular, one has to deal with products of Heaviside functions of the form $H(x)H(x) = x)H(0)$ so the value of $H(0)$ plays an important role. Here we choose $H(0) = 1/2$ in order to ensure that there exists a zero eigenvalue with associated eigensolution $(U'(x), Q'(x))$, as required by translation symmetry. However, it would be possible to develop a more rigorous treatment based on singular perturbation theory, in which the Heaviside function is treated as the high gain limit of the sigmoid function (2.4) such that $H(x) = \lim_{\to\infty} f(x)$ with $f(0) = 1/2$. Finally, note that another consequence of using a discontinuous firing rate function is that numerical bump solutions are sensitive to the effects of spatial discretization, which tend to stabilize the bump. First, writing $u(x,t) = U(x) + (x,t)$ and $q(x,t) = Q(x) + '(x,t)$ and expanding (2.1) with = 0 to first-order in (, ') leads to the linear equation

$$\frac{\partial (x,t)}{\partial t} = - (x,t) + \int_{-\infty}^{\infty} w(|x-x'|)[Q(x')H'(U(x'))-]\,dx', \tag{4.12}$$

$$\frac{\partial '(x,t)}{\partial t} = -\frac{'(x,t)}{} - Q(x)H'(U(x))-]. \tag{4.13}$$

We assume that , ' $\in L^1(\mathbf{R})$. The spectrum of the associated linear operator is found by taking $(x,t) = e^{t}(x)$ and $'(x,t) = e^{t}'(x)$ and using the identity

$$\frac{dH(U(x))}{dU} = \frac{(x)}{|U'(0)|} + \frac{(x+)}{|U'(-)|}, \tag{4.14}$$

where

$$U'(x) = \frac{1}{1+}[w(|x+|) - w(|x|)] \tag{4.15}$$

and $U'(-) = -U'(0) > 0$. Substituting into Eqs. (4.12) and (4.13) gives

$$(+1)(x) = \frac{1}{|U'(0)|}\{Q(0)(0)w(|x|) + Q(-)(-)w(|x+|)\} + \int_{-\infty}^{\infty} H(U(x'))w(|x-x'|)'(x')\,dx', \tag{4.16}$$

$$+\frac{1}{}'(x) = -\frac{}{|U'(0)|}\{Q(0)(0)(x) + Q(-)(-)(x+)\} - '(x)H(U(x))-]. \tag{4.17}$$

Let us first consider solutions (x) that vanish at $x = -$; 0 so that Eqs. (4.16) and (4.17) reduce to the simple form

$$(+1)(x) = \int_{-}^{0} w(|x-x'|)'(x')\,dx', \tag{4.18}$$

$$+\frac{1}{} + H(U(x))-]'(x) = 0. \tag{4.19}$$

There are then three possibilities: $= -1$ and $'(x) \equiv 0$; $= -1/$ and $'(x) = 0$ for $x \in [-\ ; 0]$ so that $(x) \equiv 0$; $= -1/ -$ and ' = 0 for $x \notin (-\ ; 0)$. These solutions belong to the essential spectrum since they have infinite multiplicity and do not contribute

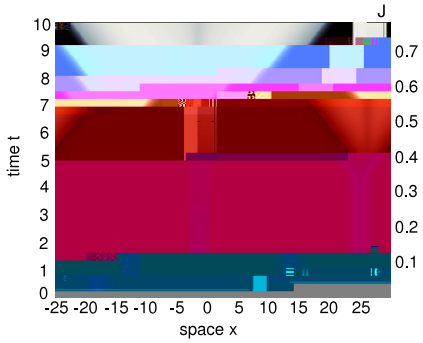

Fig. 8. Numerical simulation of an unstable stationary bump, which loses stability to a pair of counterpropagating fronts. The instability is induced by applying a burst of spatially uncorrelated Gaussian noise with amplitude = 0:01 to the entire medium at time $t = 3$. (Weak noise is required to destabilize the bump due to the discreteness of the lattice used in numerical simulations.) Parameters are = 0:1, = 20, and = 0:1.

to any instabilities. Physically speaking, they correspond to perturbations of the bump solution that do not shift the threshold crossing points. Now suppose that $.0/ \neq 0$; $.- / \neq 0$ so that the boundaries of the bump are perturbed. Eq. (4.17) implies that $'.x/$ is a linear combination of $.x/$ and $.- /$ so that $'.x/H.U.x/ - / = '.x/H.0/$. Hence,

$$+ \frac{1}{-} + H.0/ \quad '.x/ = -\frac{}{|U'.0/|}\{Q.0/ \quad .0/ \ .x/ + Q.- / \quad / \ .- / \ .x + \quad /\}:$$

Substituting for $'.x/$ in Eq. (4.16) and using Eq. (4.7) yields the eigenvalue equation

$$+ \frac{1}{-} + H.0/ \quad . \quad + 1/ \ .x/ = \frac{. \quad + 1= \ /.1 + \quad [1 - H.0/]/}{.1 + \quad /|U'.0/|}[w.|x + \quad |/ \ .- / + w.|x|/ \quad .0/]: \tag{4.20}$$

There are two classes of solutions to Eq. (4.20). The first consists of solutions of the form $.x/ = B[w.|x + |/ - w.|x|/]$ with B a constant coefficient and given by the roots of the equation

$$+ \frac{1}{-} + H.0/ \quad . \quad + 1/ = \quad + \frac{1}{-} \ .1 + \quad [1 - H.0/]/: \tag{4.21}$$

We have used the result that $|U'.0/| = .1 + \quad /^{-1}.w.0/ - w.| \quad |//$. The above equation has $_- = 0$ as a solution provided that $H.0/ = 1=2$. The zero eigenvalue is required since the full system of equations (2.1) is equivariant with respect to spatial translations, that is, the location of the center of the bump is arbitrary. The other solution is

$$_+ = . \quad - 1/\frac{}{2} - \frac{1}{-}: \tag{4.22}$$

It follows that a necessary condition for stability of the bump is that $_+ < 0$ or

$$< \frac{1}{2 \ . \quad - 1/}:$$

The other type of solution is $.x/ = B[w.|x + |/ + w.|x|/]$ with given by the roots of the equation

$$+ \frac{1}{-} + \quad =2 \quad . \quad + 1/ = \quad + \frac{1}{-} \ .1 + \quad =2/; \tag{4.23}$$

where we have set $H.0/ = 1=2$ and

$$= \frac{w.|0|/ + w.| \quad |/}{w.|0|/ - w.| \quad |/} > 1: \tag{4.24}$$

This yields the pair of eigenvalues $= b_{\pm}$, where

$$b_{\pm} = \frac{1}{2}\left(0 \quad 1 + \frac{}{2} \quad - \quad 1 + \frac{1}{-} + \frac{}{2} \quad \pm \quad s \quad 1 + \frac{}{2} \quad - .1 + 1= \quad + \quad =2/ \quad ^2 + 4 \quad \frac{1}{-} + \frac{}{2} \quad . \quad - 1/A\right): \tag{4.25}$$

Since > 1, it follows that $b_{\pm}$ are real with $b_+ > 0$ and, hence, the bump is always unstable. The unstable bump forms a separatrix between an active and an inactive homogeneous steady state, and evolves into one of these states via a pair of counterpropagating fronts. This is illustrated in Fig. 8.

5. Synchronous oscillations

Shusterman and Troy [38] have recently shown that rhythmic activity can occur in a neural field model with linear adaptation and a Heaviside firing rate function provided that the strength of negative feedback is sufficiently high, see Eqs. (1.1) and (1.2). In such a parameter regime, the space-clamped version of these equations exhibits bistability in which a stable rest state coexists with a stable limit cycle. A local stimulation of the corresponding spatially extended network can then lead to the emergence of synchronous oscillations that expand outwards, ultimately leading to synchronization of the whole network. However, since the linear form of adaptation assumed in the Pinto Ermentrout model is not directly related to physiological models of adaptation, it is difficult to determine whether or not a large value of is reasonable. Indeed, the analysis of Benda and Herz [18] suggests that the negative feedback should be proportional to the firing rate which would be nonlinear in the case of a Heaviside firing rate function. It is also possible to generate oscillations when nonlinear adaptation is included, although it appears necessary to introduce different activation thresholds for the adaptation current and spiking [40]. Here we show how synaptic depression with or without spike frequency adaptation can generate oscillations in the system given by Eq. (2.1). Such oscillations arise when the firing rate function is taken to be the piecewise linear activation function (2.3) rather than a Heaviside function.

5.1. Phase space analysis

As a means of determining the oscillatory behavior of the system, we examine the equilibria of the space-clamped system [43,41,49]

$$\begin{aligned} \dot{u}.t/ &= -u.t/ + q.t/f.u.t/ - a.t//; \\ \dot{q}.t/ &= 1 - q.t/ - \quad q.t/f.u.t/ - a.t//; \\ \dot{a}.t/ &= -a.t/ + \quad f.u.t/ - a.t//; \end{aligned} \tag{5.1}$$

where f is now taken to be the piecewise linear activation function (2.3) shown in Fig. 1. To calculate equilibria of (5.1), we consider the possible solutions on the three domains of the piecewise function $f.J/$. We find that there is a low activity or Down state on the lower domain ($u - a <$) for > 0 such that $.u; q; a/ = .0; 1; 0/$. The stability of this Down state is determined by the eigenvalues of the Jacobian

$$\mathcal{J}.0; 1; 0/ = \begin{pmatrix} -1 & 0 & 0 \\ 0 & -1= & 0 \\ 0 & 0 & -1= \end{pmatrix}! \tag{5.2}$$

and is therefore stable for all realistic parameters. We find additional equilibria by solving (5.1) on the middle and upper domains of f. On the middle domain ($\leq u - a \leq \quad + \quad ^{-1}$), where $f.J/ = \quad .J - \quad /$, we have

$$u = \quad .u - a - \quad /q; \tag{5.3}$$

$$q = 1=.1 + \quad .u - a - \quad //; \tag{5.4}$$

$$a = \quad .u - a - \quad /; \tag{5.5}$$

$$\leq u - a \leq \quad + \quad ^{-1}; \tag{5.6}$$

which has solutions

$$u = \frac{-.1 + \quad / \quad - \quad \pm\sqrt{\mathcal{D}}}{. \quad + .1 + \quad / \quad - \quad \pm\sqrt{\mathcal{D}}/} \tag{5.7}$$

$$q = \frac{2.1 + \quad /}{+.1 + \quad / \quad - \quad \pm\sqrt{\mathcal{D}}} \tag{5.8}$$

$$a = \frac{-.1 + \quad / \quad - \quad \pm\sqrt{\mathcal{D}}}{2.1 + \quad /} \tag{5.9}$$

$$\mathcal{D} = . \quad -.1 + \quad / \quad - \quad /^2 - 4 \quad .1 + \quad / \quad ; \quad = \quad ; \tag{5.10}$$

provided $\mathcal{D} \geq 0$ and condition (5.6) is satisfied. Stability is determined by the eigenvalues of the Jacobian

$$\mathcal{J}.u; q; a/ = \begin{pmatrix} -1 + \quad q & .u - a - \quad / & - \quad q \\ - \quad q \quad -.1= + & .u - a - \quad // & \quad q \quad : \\ = & 0 & -.1 + \quad /= \end{pmatrix}! \tag{5.11}$$

We find that for a wide range of parameters, the middle domain contains two equilibria, one of which is a saddle and the other is a stable or unstable spiral. The latter corresponds to a high activity or Up state. For sufficiently fast depression and/or adaptation, destabilization of the Up state can lead to the formation of a stable limit cycle via a Hopf bifurcation, see Figs. 9 and 10. In parameter regimes where the spiral equilibrium does not exist, the Up state occurs on the upper domain ($u - a > \quad + \quad ^{-1}$), where $f.J/ = 1$, and is given by

$$u = 1=.1 + \quad /; \tag{5.12}$$

$$q = 1=.1 + \quad /; \tag{5.13}$$

$$a = \quad : \tag{5.14}$$

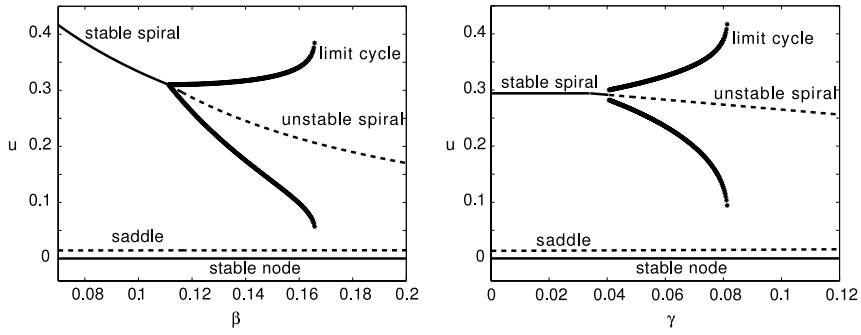

Fig. 9. (Left) Bifurcation diagram showing fixed points u of the system (5.1) as a function of . Other parameters are = 0:05, = 5, = 20, = 0:01 and = 4. Linear stability is determined using the eigenvalues of the Jacobian given by (5.11). Stable (unstable) branches are shown as solid (dashed) curves, whereas the stable limit cycle is shown as a thick solid curve. (Right) Corresponding bifurcation diagram showing u as a function of for = 0:12.

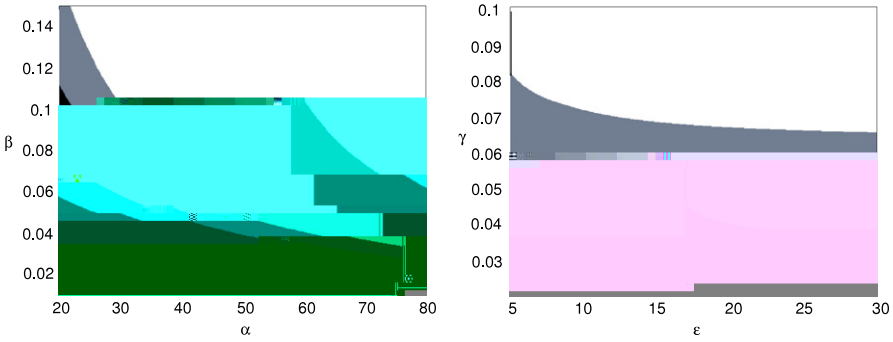

Fig. 10. (Left) Stability diagram in the (;) plane showing where the Up state is a stable spiral (black), an unstable spiral surrounded by a stable limit cycle (grey), or an unstable spiral without a limit cycle (white). (Right) Corresponding stability diagram in the (;) plane. Other parameters are as in Fig. 9.

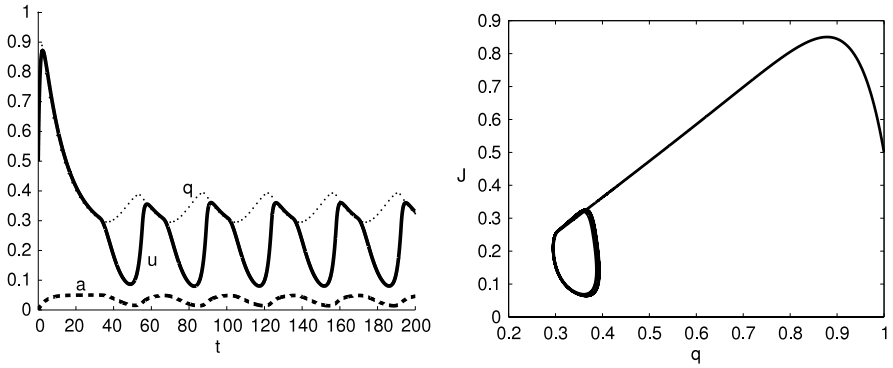

Fig. 11. Numerical simulation of the space-clamped system (5.1) using the parameters = 0:01, = 4, = 50, = 0:06, = 4, and = 0:05. (Left) Plot of u, q, and a trajectories in time. As predicted by linear stability analysis, the solution settles into a limit cycle about the Up state. (Right) A plot in the (q; J) phase plane, where $J = u - a$ is the total current input to the firing rate function $f(J)$. Notice that at its lowest point, J dips below the value corresponding to the mean value of f: $f(J) = 0:135$; $0:5$.

Its stability is determined by the eigenvalues of the Jacobian

$$\mathcal{J}(u;q;a) = \begin{pmatrix} -1 & 1 & 0 \\ 0 & -.1= & 0 \\ 0 & 0 & -1= \end{pmatrix} + \begin{pmatrix} ! & & \\ & / & \\ & & \end{pmatrix}; \tag{5.15}$$

which guarantees that such an Up state is always stable.

In Fig. 11 we show a simulation of the space-clamped network for a choice of parameters that supports a limit cycle. The parameter values are consistent with physiological measurements and previous models, for which the synaptic depression time constant is in the range 200 800 ms [24,25] and the adaptation time constant is in the range 20 80 ms [18 20]. Notice that all variables oscillate at a period of roughly 30 time units or 300 ms, which correlates nicely with the timescale of epileptiform events in slice and *in vivo* [2,6,38,3]. It also indicates that the synaptic depression timescale sets the period of oscillations in our model. Indeed, spike frequency adaptation as realized in this model does not play a major role in generating oscillations. Indeed, the network can support self-sustained oscillations in the absence of adaptation (= 0) as shown in Fig. 12. One major difference from the Pinto Ermentrout model with large negative feedback is that the equilibrium spiral in our model is associated with an Up state rather than a Down or rest state [36].

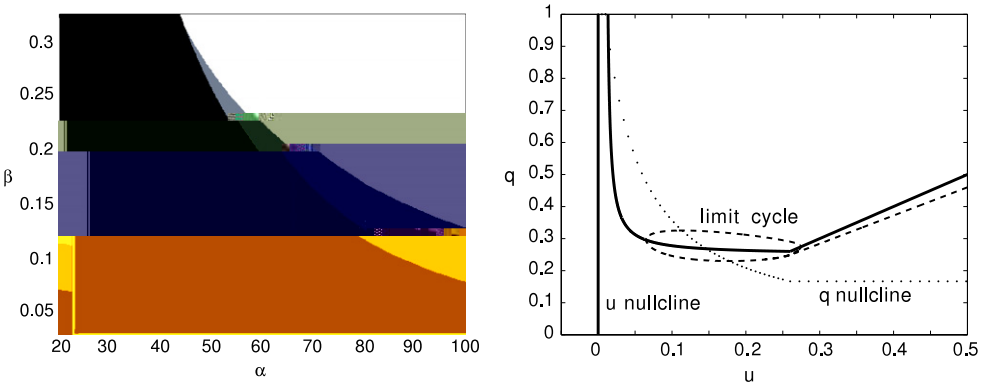

Fig. 12. (Left) Stability diagram for the space-clamped system (5.1) in the case of no adaptation (= 0), showing regions in parameter space where the Up state is a stable spiral (black), an unstable spiral surrounded by a stable limit cycle (grey), or an unstable spiral without a limit cycle (white). Other parameters are = 0:01, and = 4. (Right) Numerical simulation of (5.1) in the absence of adaptation using the parameters = 0:01, = 4, = 50, = 0:06, and = 0. We plot the trajectory of q versus u (dashed line) given the initial condition $.u; q/ = .1; 1/$. Even in the absence of adaptation, the system supports a stable limit cycle.

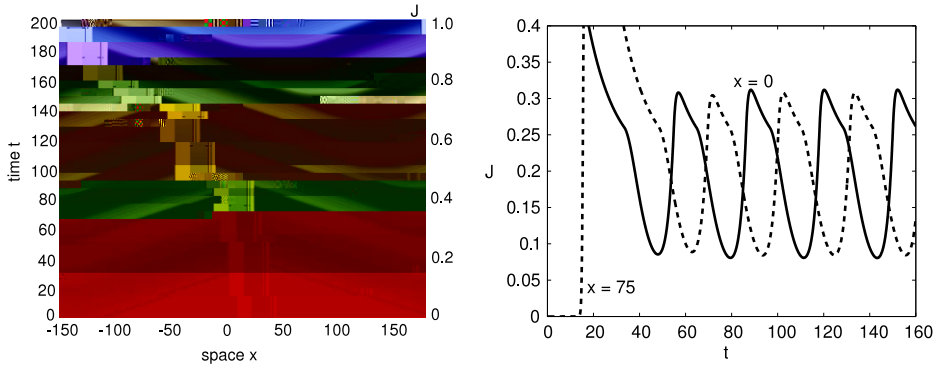

Fig. 13. Self-sustained oscillations in space. (Left) Numerical simulation of the system (2.1) when the firing rate is the piecewise linear function (2.3). An initial Gaussian activity profile evolves into a core of oscillatory activity that emits outward propagating pulses. These pulses of activity arise due to neighboring cells oscillating with a spatially-dependent phase shift. Although the baseline current is not subthreshold in the sense of causing no firing rate, it is relatively small compared to the pulse amplitude. We plot the evolution of input current J in pseudocolor as a function of space x and time t. Notice that the oscillating core is relatively confined in this long time interval and hardly expands outward at all. Parameters are = 0:01, = 50, = 0:05, = 4, and = 0:05. (Right) Corresponding trajectories of current J at two spatial locations.

5.2. Spatially extended model

A number of previous studies have shown how a space-clamped system with synaptic depression can support oscillations in population activity [43,41]. However, as far as we are aware, the evolution of self-sustained oscillations in space and time has not been explored before in such a system. Therefore, we extend the results of the previous section by examining the behavior of the full system (2.1) in the case of the piecewise linear activation function (2.3) and for the same range of parameter values for depression and adaptation as the space-clamped case. We take an initial condition in the form of a Gaussian

$$.u.x; 0/; q.x; 0/; a.x; 0// = .\mathcal{A}e^{-x^2=\ ^2}; 1; 0/; \tag{5.16}$$

where $\mathcal{A} = 0{:}5$ and = 15 are the amplitude and width of the Gaussian. We numerically solve (2.1) using fourth-order Runge Kutta with timestep $\mathcal{1}t = 0{:}01$ and Riemann integration on 4000 gridpoints for the convolution term, verifying that the time and space steps were small enough so that they did not affect the qualitative behavior. Boundary points evolve freely, and the domain is chosen to be large enough that the oscillating core is unaffected by boundaries. In Fig. 13 we show a simulation wherein an oscillating core of activity generates outward propagating pulses. Note that this self-sustaining activity does not require continuous input [31] nor does the non-dimensionalized synaptic input current go below zero [38,36,39]. As seen in the snapshots of Fig. 14, the oscillating core expands extremely slowly, remaining localized to the area of initial input on the timescale of several seconds. As mentioned above, the network supports similar behavior in the absence of spike frequency adaptation (= 0), as illustrated in Fig. 15.

Note that the system (2.1) also supports solitary traveling pulses in the case of the piecewise linear activation function (2.3). However, such pulses do not exist in the same parameter range as synchronous oscillations. Although we cannot derive rigorous conditions for the existence of traveling pulses, as we did in Section 3.2 for a Heaviside firing rate function, we can numerically simulate traveling pulses as illustrated in Fig. 15 for a pair of counter propagating waves. Similar to the traveling pulse shown in Fig. 4, a pulse is defined by the region where $J. / \geq$, and $J. / <$ otherwise. Hence, although the Heaviside firing rate function is very useful for carrying out a detailed analysis of spatiotemporal dynamics in neural field models, it cannot capture all solutions that arise when a more realistic firing rate function is considered.

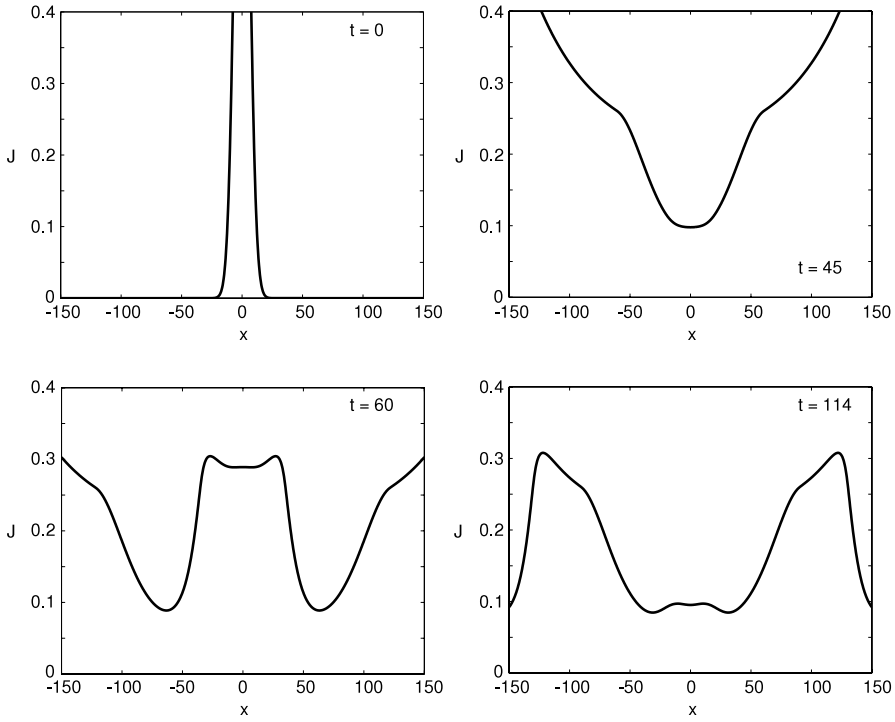

Fig. 14. Snapshots of total input current $J(x;t)$ as a function of space x for times (Top left) $t = 0$; (Top right) $t = 45$; (Bottom left) $t = 65$; and (Bottom right) $t = 139$. Oscillating core is centered at $x = 0$ and periodically emits pulses of activity after an initial traveling front.

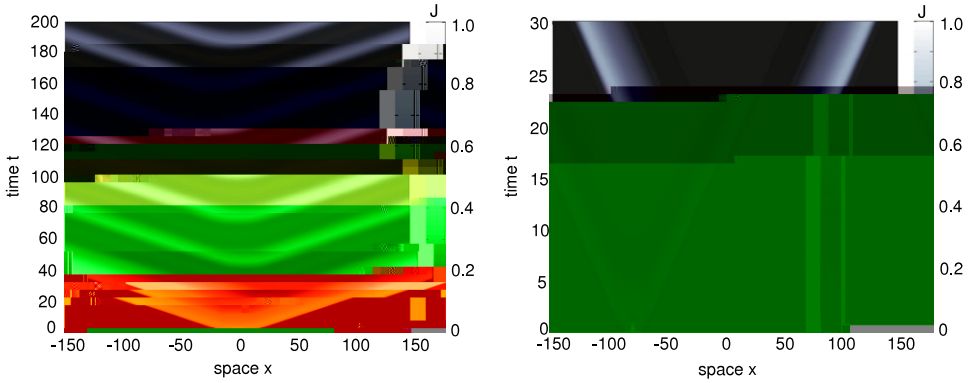

Fig. 15. (Left) Self-sustained oscillations with no adaptation. As in Fig. 13, we find a pulse-emitting core that oscillates synchronously, and in this case adaptation is not necessary to sustain these dynamics. We plot the evolution of input current J in pseudocolor as a function of space x and time t. Parameters are $= 0.01$, $= 50$, $= 0.1$, and $= 0$. (Right) Two counterpropagating pulses supported by the system (2.1) in the case where the activation function f is piecewise linear as defined in (2.3). Initial condition is taken to be the Gaussian defined in (5.16). Parameters are $= 20$, $= 0.2$, $= 0.1$, $= 5$, $= 0.01$, and $= 4$.

6. Discussion

In this paper, we analyzed the spatiotemporal dynamics of an excitatory neuronal network with two physiologically based forms of nonlinear negative feedback synaptic depression and spike frequency adaptation. Both depression and adaptation were introduced as dynamically evolving variables that depend on the output firing rate. We showed that traveling fronts and pulses exist over a reasonable range of parameters, and that adaptation plays little or no role in determining the wavespeed and pulsewidth. Stationary pulses or bumps also exist if adaptation is removed but they are unstable for a purely excitatory network. Finally, when the firing rate function is taken to be piecewise linear, self-sustained oscillations exist in the spatially extended network. A localized region of synchronous activity repetitively emits traveling pulses with each oscillation. Self-sustained oscillations and stationary superthreshold activity have been observed in real neural tissue, both in slice [2,3] and *in vivo* [3,38]. While the frequency of oscillations seems to match nicely with that observed in experiments (1 10 Hz), the spatial scale of emitted traveling pulses seems to be much longer. That is, assuming that synaptic connections have a range of 1 mm, the width of pulses ranges between 5 30 mm, whereas those in slice tend to be roughly 1 mm [29,10,5].

Our analysis suggests several future directions. First, we could use singular perturbation theory to analyze the stability of bumps in the case of a sigmoid firing rate function in the high-gain limit. This would avoid some of the problems associated with discontinuities highlighted in this paper. Second, we could examine the behavior of standing bumps as well as the self-sustained oscillatory solutions in two dimensions. In previous work, Fourier analysis has been used to predict how the symmetry of circular bumps is broken when they are perturbed [33,50,51]. Troy and Shusterman have shown that the Pinto Ermentrout model supports self-sustained oscillations in two dimensions when the symmetry of a ring wave is broken [36]. We could see if a similar mechanism exists in our model and explore

the effects of having complex eigenvalues in the Up rather than the Down state. Finally, in the space-clamped model with only synaptic depression, noise provides a means of transitioning between the Up and Down states [41]. Including noise of the appropriate form in our model could lead to interesting behavior in the spatially extended case.

Acknowledgements

This work was supported by the NSF (DMS 0813677 and RTG 0354259). We would like to thank Bill Troy (University of Pittsburgh) for highlighting the issue of finding a physiological interpretation of negative feedback in the Pinto Ermentrout model, which partly motivated the current work.

References

[1] G. Buzsaki, Rhythms of the Brain, Oxford University Press, Oxford, 2006.
[2] J.-Y. Wu, L. Guan, Y. Tsau, Propagating activation during oscillations and evoked responses in neocortical slices, J. Neurosci. 19 (12) (1999) 5005 5015.
[3] J. Milton, P. Jung, Epilepsy as a Dynamic Disease, Springer, Berlin, 2003.
[4] R.D. Chervin, P.A. Pierce, B.W. Connors, Periodicity and directionality in the propagation of epileptiform discharges across neocortex, J. Neurophysiol. 60 (5) (1988) 1695 1713.
[5] J.-Y. Wu, Propagating waves of activity in the neocortex: What they are, what they do, Neuroscientist 14 (5) (2008) 487 502.
[6] X. Huang, W.C. Troy, Q. Yang, H. Ma, C.R. Laing, S.J. Schiff, J.-Y. Wu, Spiral waves in disinhibited mammalian neocortex, J. Neurosci. 24 (44) (2004) 9897 9902.
[7] Y.W. Lam, L.B. Cohen, M. Wachowiak, M.R. Zochowski, Odors elicit three different oscillations in the turtle olfactory bulb, J. Neurosci. 20 (2) (2000) 749 762.
[8] K. Delaney, A. Gelperin, M. Fee, J. Flores, R. Gervais, D. Tank, Waves and stimulus-modulated dynamics in an oscillating olfactory network, Proc. Natl. Acad. Sci. USA 91 (1994) 669 673.
[9] J.C. Prechtl, L.B. Cohen, B. Pesaran, P.P. Mitra, D. Kleinfeld, Visual stimuli induce waves of electrical activity in turtle cortex, Proc. Natl. Acad. Sci. USA 94 (14) (1997) 7621 7626.
[10] W. Xu, X. Huang, K. Takagaki, J.-Y. Wu, Compression and reflection of visually evoked cortical waves, Neuron 55 (1) (2007) 119 129.
[11] A. Benucci, R. Frazor, M. Carandini, Standing waves and traveling waves distinguish two circuits in visual cortex, Neuron 55 (2007) 103 117.
[12] F. Han, N. Caporale, Y. Dan, Reverberation of recent visual experience in spontaneous cortical waves, Neuron 60 (2) (2008) 321 327.
[13] C.C.H. Petersen, A. Grinvald, B. Sakmann, Spatiotemporal dynamics of sensory responses in layer 2/3 of rat barrel cortex measured in vivo by voltage-sensitive dye imaging combined with whole-cell voltage recordings and neuron reconstructions, J. Neurosci. 23 (4) (2003) 1298 1309.
[14] D. Rubino, K.A. Robbins, N.G. Hatsopoulos, Propagating waves mediate information transfer in the motor cortex, Nat. Neurosci. 9 (12) (2006) 1549 1557.
[15] X.J. Wang, Synaptic basis of cortical persistent activity: The importance of NMDA receptors to working memory, J. Neurosci. 19 (21) (1999) 9587 9603.
[16] U. Lee, S. Kim, K.-Y. Jung, Classification of epilepsy types through global network analysis of scalp electroencephalograms, Phys. Rev. E 73 (4) (2006) 041920.
[17] G.B. Ermentrout, D. Kleinfeld, Traveling electrical waves in cortex: Insights from phase dynamics and speculation on a computational role, Neuron 29 (1) (2001) 33 44.
[18] J. Benda, A.V.M. Herz, A universal model for spike-frequency adaptation, Neural Comput. 15 (11) (2003) 2523 2564.
[19] D.V. Madison, R.A. Nicoll, Control of the repetitive discharge of rat CA1 pyramidal neurones in vitro, J. Physiol. 354 (1984) 319 331.
[20] M. Stocker, M. Krause, P. Pedarzani, An apamin-sensitive Ca^{2+}-activated K^{+} current in hippocampal pyramidal neurons, Proc. Natl. Acad. Sci. USA 96 (8) (1999) 4662 4667.
[21] B. Ermentrout, Linearization of f-I curves by adaptation, Neural Comput. 10 (7) (1998) 1721 1729.
[22] X.J. Wang, Calcium coding and adaptive temporal computation in cortical pyramidal neurons, J. Neurophysiol. 79 (3) (1998) 1549 1566.
[23] R.S. Zucker, W.G. Regehr, Short term synaptic plasticity, Ann. Rev. Physiol. 64 (2) (2002) 355 405.
[24] L.F. Abbott, J.A. Varela, K. Sen, S.B. Nelson, Synaptic depression and cortical gain control, Science 275 (5297) (1997) 220 224.
[25] M.V. Tsodyks, H. Markram, The neural code between neocortical pyramidal neurons depends on neurotransmitter release probability, Proc. Natl. Acad. Sci. USA 94 (2) (1997) 719 723.
[26] M. Tsodyks, K. Pawelzik, H. Markram, Neural networks with dynamic synapses, Neural Comput. 10 (4) (1998) 821 835.
[27] C. Stevens, J. Wesseling, Activity-dependent modulation of the rate at which synaptic vesicles become available to undergo exocytosis, Neuron 21 (1998) 415 424.
[28] S. Brenowitz, L.O. Trussell, Minimizing synaptic depression by control of release probability, J. Neurosci. 21 (6) (2001) 1857 1867.
[29] D.J. Pinto, G.B. Ermentrout, Spatially structured activity in synaptically coupled neuronal networks: I. Traveling fronts and pulses, SIAM J. Appl. Math. 62 (1) (2001) 206 225.
[30] D.J. Pinto, G.B. Ermentrout, Spatially structured activity in synaptically coupled neuronal networks: II. Lateral inhibition and standing pulses, SIAM J. Appl. Math. 62 (1) (2001) 226 243.
[31] S.E. Folias, P.C. Bressloff, Breathing pulses in an excitatory neural network, SIAM J. Appl. Dyn. Syst. 3 (3) (2004) 378 407.
[32] S.E. Folias, P.C. Bressloff, Stimulus-locked traveling waves and breathers in an excitatory neural network, SIAM J. Appl. Math. 65 (6) (2005) 2067 2092.
[33] S.E. Folias, P.C. Bressloff, Breathers in two-dimensional neural media, Phys. Rev. Lett. 95 (20) (2005) 208107.
[34] S. Coombes, Waves, bumps, and patterns in neural field theories, Biol. Cybern. 93 (2) (2005) 91 108.
[35] C.R. Laing, Spiral waves in nonlocal equations, SIAM J. Appl. Dyn. Syst. 4 (3) (2005) 588 606.
[36] W.C. Troy, V. Shusterman, Patterns and features of families of traveling waves in large-scale neuronal networks, SIAM J. Appl. Dyn. Syst. 6 (1) (2007) 263 292.
[37] Z.P. Kilpatrick, S.E. Folias, P.C. Bressloff, Traveling pulses and wave propagation failure in inhomogeneous neural media, SIAM J. Appl. Dyn. Syst. 7 (1) (2008) 161 185.
[38] V. Shusterman, W.C. Troy, From baseline to epileptiform activity: A path to synchronized rhythmicity in large-scale neural networks, Phys. Rev. E 77 (6) (2008) 061911.
[39] W.C. Troy, Traveling waves and synchrony in an excitable large-scale neuronal network with asymmetric connections, SIAM J. Appl. Dyn. Syst. 7 (4) (2008) 1247 1282.
[40] S. Coombes, M.R. Owen, Bumps, breathers, and waves in a neural network with spike frequency adaptation, Phys. Rev. Lett. 94 (14) (2005) 148102.
[41] E. Bart, S. Bao, D. Holcman, Modeling the spontaneous activity of the auditory cortex, J. Comput. Neurosci. 19 (3) (2005) 357 378.
[42] V. Matveev, X.J. Wang, Implications of all-or-none synaptic transmission and short-term depression beyond vesicle depletion: A computational study, J. Neurosci. 20 (4) (2000) 1575 1588.
[43] J. Tabak, W. Senn, M.J. O'Donovan, J. Rinzel, Modeling of spontaneous activity in developing spinal cord using activity-dependent depression in an excitatory network, J. Neurosci. 20 (8) (2000) 3041 3056.
[44] S. Amari, Dynamics of pattern formation in lateral-inhibition type neural fields, Biol. Cybern. 27 (2) (1977) 77 87.
[45] O. Faugeras, R. Veltz, F. Grimbert, Persistent neural states: Stationary localized activity patterns in nonlinear continuous n-population, *q*-dimensional neural networks, Neural Comput. 21 (2009) 147 187.
[46] Y. Guo, C.C. Chow, Existence and stability of standing pulses in neural networks: I. Existence, SIAM J. Appl. Dyn. Syst. 4 (2) (2005) 217 248.
[47] Y. Guo, C.C. Chow, Existence and stability of standing pulses in neural networks: II. Stability, SIAM J. Appl. Dyn. Syst. 4 (2) (2005) 249 281.
[48] J. Rubin, A. Bose, Localized activity patterns in excitatory neuronal networks, Network 15 (2) (2004) 133 158.
[49] B.B. Vladimirski, J. Tabak, M.J. ODonovan, J. Rinzel, Episodic activity in a heterogeneous excitatory network, from spiking neurons to mean field, J. Comput. Neurosci. 25 (2008) 39 63.
[50] M.R. Owen, C.R. Laing, S. Coombes, Bumps and rings in a two-dimensional neural field: Splitting and rotational instabilities, New J. Phys. 9 (2007) 378.
[51] C.R. Laing, W.C. Troy, PDE methods for nonlocal models, SIAM J. Appl. Dyn. Syst. 2 (3) (2003) 487 516.